JAMES | Journal of Advances in Modeling Earth Systems

RESEARCH ARTICLE
10.1029/2018MS001538

Modeling Neodymium Isotopes in the Ocean Component of the Community Earth System Model (CESM1)

Sifan Gu[1,2], Zhengyu Liu[3], Alexandra Jahn[4], Johannes Rempfer[5], Jiaxu Zhang[6], and Fortunat Joos[5]

[1]Department of Atmospheric and Oceanic Sciences, University of Wisconsin-Madison, Madison, WI, USA, [2]Now at Physical Oceanography Laboratory, Ocean University of China, Qingdao, China, [3]Atmospheric Science Program, Department of Geography, The Ohio State University, Columbus, OH, USA, [4]Department for Atmospheric and Oceanic Sciences and Institute of Arctic and Alpine Research, University of Colorado Boulder, Boulder, CO, USA, [5]Climate and Environmental Physics, Physics Institute and Oeschger Center for Climate Change Research, University of Bern, Bern, Switzerland, [6]Computational Physics and Methods (CCS-2) and Center for Nonlinear Studies (CNLS), Los Alamos National Laboratory, Los Alamos, NM, USA

Abstract Neodymium (Nd) isotopic composition (ε_{Nd}) is an important tracer for water mass mixing and the reconstruction of past ocean circulation. To allow for a direct model-data comparison, we have implemented Nd isotopes in the ocean component of the Community Earth System Model (CESM1.3). The model is able to capture the major features of the observed modern distribution of both ε_{Nd} and Nd concentrations. Our model provides a useful tool for the interpretation of ε_{Nd} reconstructions. For example, we show that in an idealized North Atlantic freshwater hosing experiment, ε_{Nd} changes in the Atlantic are documenting primarily the changes in water mass mixing and are hardly affected by the concomitant and large changes in the marine biological productivity and organic matter fluxes. However, the hosing experiment also shows that the end-member changes due to the change of ocean circulation can influence the interpretation of ε_{Nd} in the Atlantic, depending on the location. The implementation of Nd, together with other existing tracers, such as $\delta^{18}O$, $^{231}Pa/^{230}Th$, $\delta^{13}C$, and radiocarbon in the same model, can improve our understanding of past ocean circulation significantly.

Plain Language Summary The Climate model is an important tool to study past climate. However, previous model-data comparison suffers from indirect comparison since reconstructions measures proxy records and climate model simulate physical variables, both of which have uncertainties and it is hard to address the model data discrepancies. To meet this challenge, we implement the Nd isotopes, which is more and more used in paleoceanography, in the ocean component of the Community Earth System Model (CESM). Our model is able to simulate ε_{Nd} in good agreement with observations. With other isotopes, such as $\delta^{18}O$, $^{231}Pa/^{230}Th$, $\delta^{13}C$, and radiocarbon in the same model, this isotope-enabled CESM provides a powerful tool to improve the understanding of past ocean circulation changes. Furthermore, the hosing experiment suggests that the interpretation of ε_{Nd} changes in the Atlantic as changes in the water mass mixing can be complicated by the changes in the end-member values in some locations.

Key Points:
- Nd isotopes are implemented in the CESM1, which simulate the Nd concentration and ε_{Nd} in reasonable agreement with observations
- In idealized water hosing experiment, ε_{Nd} changes in the Atlantic mainly reflect changes in the mixing between different water masses
- End-member changes due to the change of ocean circulation can influence the interpretation of ε_{Nd} in some locations

Supporting Information:
- Supporting Information S1

Correspondence to:
S. Gu,
gusifan@gmail.com

Citation:
Gu, S., Liu, Z., Jahn, A., Rempfer, J., Zhang, J., & Joos, F. (2019). Modeling neodymium isotopes in the ocean component of the community earth system model (CESM1). *Journal of Advances in Modeling Earth Systems*, *11*, 624–640. https://doi.org/10.1029/2018MS001538

Received 23 OCT 2018
Accepted 7 FEB 2019
Accepted article online 11 FEB 2019
Corrected 13 MAR 2019
Published online 4 MAR 2019

This article was corrected on 13 MAR 2019. See the end of the full text for details.

1. Introduction

Neodymium (Nd), as a rare earth element, is an important tracer in paleoceanographic studies. The main sources and sinks of Nd in the ocean are from dust deposition, riverine input, boundary exchange, and reversible scavenging. Neodymium isotopic composition (ε_{Nd}) is reported as Nd isotopic ratio (IR, $^{143}Nd/^{144}Nd$) relative to the value of the bulk earth ($(^{143}Nd/^{144}Nd)_{CHUR} = 0.512638$; Jacobsen & Wasserburg, 1980),

$$\varepsilon_{Nd} = \left[\frac{\left(\frac{^{143}Nd}{^{144}Nd}\right)_{sample}}{\left(\frac{^{143}Nd}{^{144}Nd}\right)_{CHUR}} - 1\right] \times 10^4 .$$

ε_{Nd} is a quasi-conservative water mass tracer (Goldstein & Hemming, 2003; Jeandel, 1993) and has been used to reconstruct water mass source in paleoceanographic studies (e.g., Huang et al., 2014; Pahnke et al., 2008; Piotrowski et al., 2012; Roberts et al., 2010). The ε_{Nd} values of water masses originating from different ocean basins are distinctly different due to the different ages of continental crusts in different regions and the related differences in isotopic source fluxes to the ocean: the North Atlantic features some of the most negative ε_{Nd} values recorded, while the North Pacific has

generally less negative ε_{Nd} values compared to the North Atlantic. Strongly negative ε_{Nd} values are linked to Nd sources from old continental crust material, for example, as found in North America and Scandinavia, and termed "unradiogenic", whereas ε_{Nd} values close to that of bulk earth are linked to Nd sources from relatively young continental crust material and termed "radiogenic". In the modern ocean, a typical value of ε_{Nd} is ~−13.5 for the North Atlantic Deep Water (NADW), ~−8.5 for the Antarctic Intermediate Water (AAIW) and the Antarctic Bottom Water (AABW), and ~−3.5 for water from the deep Pacific (Amakawa et al., 2009; Piepgras & Wasserburg, 1987; Stichel et al., 2012). In the Atlantic basin, ε_{Nd} covaries with salinity and tends to trace different water masses (von Blanckenburg, 1999). Unlike proxies such as $\delta^{13}C$ and $^{231}Pa/^{230}Th$, which are also used to reconstruct past ocean circulation but are subject to biological processes, ε_{Nd} is suggested to be minimally influenced by biological processes (Goldstein & Hemming, 2003). Therefore, it is important to implement Nd isotopes into climate models to help improve our understanding of ocean circulation.

The interpretation of the reconstructed ε_{Nd} changes in the Atlantic as water mass mixing changes is based on the assumption that ε_{Nd} end-member changes can be neglected (e.g., Piotrowski et al., 2004). However, NADW is formed by very unradiogenic Labrador Sea Water (<−20) and relative radiogenic water from the Norwegian and Greenland Sea (−7 to −10; Goldstein & Hemming, 2003). Uncertainty in the relative contributions from these different deepwater formation regions in the past (Crocket et al., 2011; Dokken & Jansen, 1999; Labeyrie et al., 1992) leads to uncertainties in the ε_{Nd} end-member value of NADW (van de Flierdt et al., 2016), complicating the interpretation of ε_{Nd} reconstructions. Determining to which extent the ε_{Nd} end-member values may have changed in different source regions and understanding the underlying mechanisms are of great interest to the paleoceanographic community.

The Nd isotopes have already been simulated in modeling studies. These studies differ in the complexity of the applied ocean model, of the Nd isotope implementation, and of the particle field as discussed below. The first implementations of Nd isotopes were done in simple box models (Bertram & Elderfield, 1993; van de Flierdt et al., 2004; Tachikawa et al., 2003). Later, ε_{Nd} was implemented as a single, passive and conservative tracer in offline ocean circulation models (Arsouze et al., 2007; Arsouze et al., 2008; Jones et al., 2008). Jones et al. (2008) prescribed surface ε_{Nd} and did not consider external sources; these authors find that observed ε_{Nd} values are consistent with quasi-conservative water mass mixing in many regions and they postulate the need of a radiogenic Nd source in the deepwaters of the Pacific. Arsouze et al. (2007, 2008) considered the boundary exchange in the continental margins as the only source and sink for ε_{Nd}, showing the importance of boundary exchange for modeling ε_{Nd}. However, the implementation of ε_{Nd} in Jones et al. (2008) and Arsouze et al. (2007, 2008) are simplified, as ε_{Nd} represents an IR and a ratio does not correspond to a conservative tracer during transport and water mass mixing. Also, their model did not permit a full assessment of the entire Nd cycle or an investigation of the spatial pattern of Nd concentration. Therefore, later studies (Arsouze et al., 2009; Rempfer et al., 2011; Siddall et al., 2008) simulated ^{143}Nd and ^{144}Nd as two explicit tracers with all major Nd sources and sinks considered, and, importantly, including the reversible scavenging of dissolved Nd by sinking particles. Siddall et al. (2008), pioneering the reversible scavenging approach, used an offline transport matrix of the MIT general circulation model with prescribed surface boundary condition of ε_{Nd} and Nd concentration and prescribed particle fields and fluxes for biogenic opal, calcium carbonate, particulate organic carbon (POC), and dust. Their work showed the important role of reversible scavenging of Nd isotopes by particles in the oceanic cycle of Nd. However, Siddall et al. (2008) did not explicitly include Nd exchange at continental boundaries. Arsouze et al. (2009) were the first to use a fully prognostic coupled dynamic and biogeochemical model to simulate ε_{Nd} and Nd concentrations. Furthermore, their approach explicitly considered different sources and sinks of Nd: dust sources, river sources, boundary exchanges, and reversible scavenging. They showed that boundary exchanges are the dominant source but that dust and river sources are also important, for both surface and subsurface waters. However, due to the high computational cost of their model, the magnitude of different sources, and the partition coefficient of particles could not be optimized through sensitivity tests. Rempfer et al. (2011) extended the earlier work by Siddall et al. (2008) and Arsouze et al. (2009) by performing a comprehensive investigation of Nd sources and the particle partition coefficient in a frictional-geostrophic balance ocean model with coarse resolution. This cost-efficient model allowed for extensive sensitivity experiments for model calibration. In Rempfer et al. (2012a), the effect of changes in the overturning circulation on ε_{Nd} was examined, showing that

variations in ε_{Nd} reflect the changes in the formation of NADW and AABW and that changes in ε_{Nd} of end-members are relatively small. However, this conclusion may be affected by the relatively coarse resolution and the simplified ocean dynamics of the applied ocean model.

Here, we describe the implementation of ^{143}Nd and ^{144}Nd in a comprehensive earth system model that accounts for different deepwater source regions in the North Atlantic and perform a detailed investigation of changes in the end-member signature in response to ocean circulation and climate change. Both of these address gaps left by the previous studies, all of which were performed in much simpler ocean models and/or used much simpler source functions. In particular, we have implemented Nd isotopes in the ocean component of the Community Earth System Model (CESM1), following the modeling schemes of Arsouze et al. (2009), Rempfer et al. (2011), and Siddall et al. (2008). We implemented two versions of Nd isotopes: one is a standard Nd isotope, which uses the particle fluxes simultaneously calculated by the marine biogeochemical module (*p*-coupled Nd), similar to the Nd in Arsouze et al. (2009) and Rempfer et al. (2011); the other is a Nd isotope with prescribed particle fluxes (*p*-fixed Nd). With these two versions of Nd in the same model, we are able to study the potential influence of biological productivity change on ε_{Nd} distribution by comparing the *p*-coupled ε_{Nd} and *p*-fixed ε_{Nd}. The *p*-fixed version also provides a computationally efficient tool for sensitivity studies. To study how ε_{Nd} end-member values will respond to the changes in the NADW formation, we performed and analyzed a freshwater water hosing experiment in the North Atlantic.

This paper describes the details of Nd isotopes in the CESM1. Our main objective is to document the implementation of Nd in the ocean component of CESM for future community references and to show the important effect of change of NADW formation on ε_{Nd} in the Atlantic and the end-member signature in a freshwater hosing experiment, which has not previously been shown. The paper is arranged as follows. In section 2, we describe the implementation of Nd isotopes and the experimental design. In section 3, we compare simulated Nd concentration and ε_{Nd} with observations and analyze the ε_{Nd} response to freshwater forcing in the North Atlantic.

2. Methods

2.1. Neodymium Isotope Implementation in CESM1

We implemented Nd isotopes (^{143}Nd and ^{144}Nd) in the ocean model (POP2; Danabasoglu et al., 2012) of the CESM version 1.3 (Hurrell et al., 2013), which is a state-of-the-art coupled climate model, used frequently for both present-day and paleoclimate research. Specific Nd model formulations, values of nontuned parameters and the model tuning approach are similar to Rempfer et al. (2011) but implemented here in a more complex physical ocean model.

The sources of Nd to the ocean stem from dust deposition, river input, and weathering of continental crust material. The surface dust deposition (F_{dust}) is prescribed using the monthly output from a model simulation by Luo et al. (2003). The annual dust deposition field is shown in Figure S1. We assume that the Nd concentration (C_{dust}) in the dust is 20 μg/g (Goldstein et al., 1984; Grousset et al., 1988, 1998), of which 2% (β_{dust}) is dissolved in ocean waters (Greaves et al., 1994). Therefore, the dust source (S_{dust}) per unit water volume in the surface layer is calculated as

$$S_{dust}(i,j,1) = \frac{F_{dust}(i,j) \times C_{dust} \times \beta_{dust}}{dz(1)}, \quad (1)$$

where *i* is the index for latitude, *j* is the index for longitude, and dz(1) is the thickness of the surface layer, which is 10 m in the model. We use the simulated river runoff (ROFF) from the coupler of CESM as river discharge. The Nd concentration (C_{river}) in the river discharge is prescribed following Goldstein and Jacobsen (1987), with 30% (γ_{river}) of Nd in the river runoff allowed to enter the ocean through estuaries (Rempfer et al., 2011). Consequently, the river source (S_{river}) is calculated as

$$S_{river}(i,j,1) = \frac{\mathrm{ROFF}(i,j) \times C_{river} \times \gamma_{river}}{dz(1)} \quad (2)$$

A boundary source is applied to the continental margin, in the upper 3,000 m of the ocean, following previous studies (Arsouze et al., 2009; Rempfer et al., 2011). The depth dependence of the boundary

source is still in debate as observed evidence remains incomplete (Howe et al., 2016; Rousseau et al., 2015; van de Flierdt et al., 2016). In our model, a given amount of Nd enters each model grid cell that is adjacent to sediments of the continental margins. We neglect the comparably small lateral grid cell areas and consider only the horizontal, bottom areas of the deepest grid cells in the upper 3,000 m for the boundary source calculation. The boundary source per unit area was treated as depth dependent in Arsouze et al. (2009) but was assumed as depth-independent in Rempfer et al. (2011). In this study, we follow Rempfer et al. (2011) and assume a globally uniform constant value for the boundary source per unit area. As in Rempfer et al. (2011), the total ocean boundary source (f_{boundary}) is a tuning parameter. The boundary source per unit water volume (S_{boundary}) for each near-bottom grid cell in the upper 3,000 m is calculated as

$$S_{\mathrm{boundary}}(i,j,k) = f_{\mathrm{boundary}} \times \frac{A(i,j,k)}{A_{tot}} \times \frac{1}{A(i,j,k) \times \mathrm{d}z(k)} = \frac{f_{\mathrm{boundary}}}{A_{\mathrm{tot}}} \times \frac{1}{\mathrm{d}z(k)} \tag{3}$$

where i, j, and k are the indices of the model grid for longitude, latitude, and depth; dz(k) is the thickness of layer k. $A(i,j,k)$ represents the bottom area of the grid cell, and A_{tot} is the total area of the continental margin in the model.

^{143}Nd and ^{144}Nd are simulated as two tracers in the model (equation (4)). ^{143}Nd and ^{144}Nd account for 36% of total Nd. Individual fluxes for ^{143}Nd and ^{144}Nd are calculated using the IR (equation (5)). The IR in the dust source is prescribed following Tachikawa et al. (2003; Figure S2). IR in the river source and the boundary source is prescribed following Jeandel et al. (2007; Figure S3). The prescribed IR in the river and boundary source features quite different values in the deepwater formation regions in the North Atlantic: most unradiogenic values (~−30) in the Labrador Sea, most radiogenic values (~3) around Iceland, and intermediate values (~−15) around the American and Scandinavian continent.

$$Nd = {}^{143}Nd + {}^{144}Nd \tag{4}$$

$$IR = {}^{143}Nd / {}^{144}Nd \tag{5}$$

The internal cycling of Nd is modeled using the reversible scavenging by sinking particles (Bacon & Anderson, 1982; Henderson et al., 1999; Siddall et al., 2005). Unlike the quasi-conservative behavior of $\varepsilon_{\mathrm{Nd}}$, the Nd concentration shows a nutrient-like distribution: it increases with depth and along the circulation pathway, due to reversible scavenging (Siddall et al., 2008). Reversible scavenging describes the adsorption and desorption of the isotopes onto sinking particles. The Nd associated with the particles that reaches the ocean bottom is buried in the sediment. This burial of Nd represents a sink which in equilibrium balances the input of Nd to the ocean from the external sources. The particles involved in the reversible scavenging of Nd are $CaCO_3$, opal, POC, and dust. The particle fluxes can be computed by the biogeochemical module (p-coupled Nd). For simplicity and computational efficiency, the particle fluxes can also be prescribed using those generated by the biogeochemical module under modern climate (p-fixed Nd). The reversible scavenging scheme in this study is the same as the scheme applied to model ^{231}Pa and ^{230}Th in the CESM (Gu & Liu, 2017). The $CaCO_3$, opal, and POC fluxes produced by the biogeochemical module in the CESM are in reasonable agreement with the observations (Gu & Liu, 2017). The dust flux is prescribed using the output from Luo et al. (2003).

The reversible scavenging (S_{rs}) considers total Nd ($[\mathrm{Nd}]_t^i$), where i denotes ^{143}Nd and ^{144}Nd, as dissolved Nd ($[\mathrm{Nd}]_d^i$) and particulate Nd ($[\mathrm{Nd}]_p^i$) associated with different particle types ($[\mathrm{Nd}]_{p,j}^i$, where j denotes to $CaCO_3$, opal and POC, and dust (equation (6)).

$$[\mathrm{Nd}]_t^i = [\mathrm{Nd}]_d^i + [\mathrm{Nd}]_p^i = [\mathrm{Nd}]_d^i + \sum_j [\mathrm{Nd}]_{p,j}^i \tag{6}$$

We assume $[\mathrm{Nd}]_{\mathrm{d}}$ and $[\mathrm{Nd}]_{\mathrm{p}}$ to be in equilibrium, and the ratio between $[\mathrm{Nd}]_{\mathrm{d}}$ and $[\mathrm{Nd}]_{\mathrm{p}}$ is controlled by the partition coefficient (K) and the ratio (R_j) between particle concentration (C_j) and the density of seawater (1,024.5 kg/m^3; equation (7)). K_j is calculated from the global average of R_j and the tuning parameter ($\frac{[Nd]_p}{[Nd]_d}$; equation (8)). Although the tuning parameter ($\frac{[Nd]_p}{[Nd]_d}$) is assumed to be the same for different particles, R_j

depends on the particle type. Therefore, K_j is different for different particles (Table 1). The tuning parameter $\frac{[Nd]_p}{[Nd]_d}$ measures the average scavenging ability in the model. Larger $\frac{[Nd]_p}{[Nd]_d}$ will lead to a reduced Nd residence time, a reduced Nd concentration and an increased interbasin ε_{Nd} contrast (Rempfer et al., 2011). We assume that there is no differentiation during the reversible scavenging and apply the same K_j to ^{143}Nd and ^{144}Nd due to their similar molecular mass. Reversible scavenging transports $[Nd]_p$ downward by the settling velocity (w) of 1,000 m/year (Arsouze et al., 2009; Dutay et al., 2009; Kriest, 2002; Rempfer et al., 2011; equation (9)). By combining equations (6) and (7), we obtain $[Nd]_p$ (equation (10)). As mentioned above, $[Nd]_p$ is removed from the ocean in the bottom layer.

$$\frac{[\mathrm{Nd}]^i_{j,p}}{[\mathrm{Nd}]^i_d} = K^i_j \times R_j \tag{7}$$

$$K_j = \left(\frac{[\mathrm{Nd}]_p}{[\mathrm{Nd}]_d}\right) \times \frac{1}{R_{j,\mathrm{avg}}} \tag{8}$$

$$S_{\mathrm{rs}} = -\frac{\partial\left(w[\mathrm{Nd}]_p\right)}{\partial z} \tag{9}$$

$$[\mathrm{Nd}]^i_p = [\mathrm{Nd}]^i_t \times \left(1 - \frac{1}{1 + \sum_j K^i_j \times R_j}\right) \tag{10}$$

The total conservation equation for Nd can be written as

$$\frac{\partial [\mathrm{Nd}]^i_t}{\partial t} = S^i_{\mathrm{dust}} + S^i_{\mathrm{river}} + S^i_{\mathrm{boundary}} + S^i_{\mathrm{rs}} + \mathrm{Transport} \tag{11}$$

In this implementation, the sources of Nd in the CESM are the dust source, the river source, and the boundary source. The sink is the reversible scavenging by particles to the ocean floor. Recent studies suggest that nepheloid layer may be important to simulate particle reactive tracers (Deng et al., 2014; Hayes et al., 2015; Rempfer et al., 2017; van de Flierdt et al., 2016). However, currently, the nepheloid layer, and hence its effect on Nd, is not modeled in the CESM.

2.2. Experiments

All the experiments in this study were run in the ocean-alone setup, forced by climatological atmospheric variables from the data set of the Coordinated Ocean-ice Reference Experiments, phase II (Large & Yeager, 2008). Our model is the low-resolution POP2 with a nominal 3° horizontal resolution and 60 vertical layers.

Our tuning procedure largely follows that of Rempfer et al. (2011). We first tuned the model parameters (f_{boundary} and $\frac{[Nd]_p}{[Nd]_d}$) in p-fixed Nd, following the method in Rempfer et al. (2011). The observations used to tune the parameters were compiled by van de Flierdt et al. (2016). This compilation has more than twice the observations than an earlier compilation (Lacan et al., 2012) used in Rempfer et al. (2011). The locations of these observations can be found in Figure 1 in van de Flierdt et al. (2016). The details of the tuning process and the sensitivity of our model to variations in f_{boundary} and $\frac{[Nd]_p}{[Nd]_d}$ are similar to Rempfer et al. (2011) and are described briefly in the supplementary information. The values of f_{boundary} and $\frac{[Nd]_p}{[Nd]_d}$ tuned for the CESM (control experiment, CTRL) are 4×10^9 g/year and 0.0009, which are similar to the values used in Rempfer et al. (2011; 5.5×10^9 g/year and 0.001, respectively). With the tuned values of f_{boundary} and $\frac{[Nd]_p}{[Nd]_d}$, the CESM simulates both Nd concentrations and ε_{Nd} in good agreement with the observations in van de Flierdt et al., 2016, as shown in section 3. A p-coupled CTRL with the same tuned parameters was also performed. The CTRL experiment is integrated for 4,000 years and has reached equilibrium. Results shown in section 3 are the decadal means at the end of CTRL.

Table 1
Variables, Abbreviations, Values, and Units in Nd Implementation

Variable	Symbol	Value	Units
Dust source density	S_{dust}		$g{\cdot}m^{-3}{\cdot}s^{-1}$
River source density	S_{river}		$g{\cdot}m^{-3}{\cdot}s^{-1}$
Boundary source density	$S_{boundary}$		$g{\cdot}m^{-3}{\cdot}s^{-1}$
Reversible Scavenging	S_{rs}		$g{\cdot}m^{-3}{\cdot}s^{-1}$
Surface dust deposition	F_{dust}		$g{\cdot}m^{-2}{\cdot}s^{-1}$
Nd concentration in dust	C_{dust}	20	μg/g
Nd release rate in dust	β_{dust}	2%	
Total dust source	f_{dust}	2.1×10^{8}	g/year
River discharge	ROFF		$kg{\cdot}m^{-2}{\cdot}s^{-1}$
Nd concentration in river	C_{river}		g/kg
Nd enters the ocean through estuaries	γ_{river}	30%	
Total river source	f_{river}	1.3×10^{9}	g/year
Total boundary source	$f_{boundary}$	4×10^{9}	g/year
Total area of continental margin	A_{tot}		m^2
Isotopic ratio	IR		
Dissolved Nd	$[Nd]_d$		pmol/kg
Particle related Nd	$[Nd]_p$		pmol/kg
Total Nd	$[Nd]_t$		pmol/kg
Ratio between $[Nd]_p$ and $[Nd]_d$	$\frac{[Nd]_p}{[Nd]_d}$	0.0009	
Particle settling velocity	w	1000	m/year
Ratio between average POC concentration and density of seawater	$R_{POC,\ avg}$	2.6×10^{-9}	
Ratio between average $CaCO_3$ concentration and density of seawater	$R_{CaCO3,\ avg}$	9.3×10^{-9}	
Ratio between average opal concentration and density of seawater	$R_{opal,\ avg}$	8.1×10^{-9}	
Ratio between average dust concentration and density of seawater	$R_{dust,\ avg}$	1.2×10^{-9}	
Partition coefficient	K		
Partition coefficient for POC	K_{POC}	3.5×10^{5}	
Partition coefficient for $CaCO_3$	K_{CaCO3}	9.7×10^{4}	
Partition coefficient for opal	K_{opal}	1.1×10^{5}	
Partition coefficient for dust	K_{dust}	7.5×10^{5}	

Note. POC = particulate organic carbon.

To test the ε_{Nd} response to the change of the Atlantic Meridional Overturning Circulation (AMOC) strength and to study whether the associated productivity change will influence the ε_{Nd} distribution in the Atlantic, we ran an idealized freshwater forcing experiment (HOSING) in both the *p*-fixed and *p*-coupled Nd model setup. The HOSING experiment is forced by a freshwater flux of 1 Sv to 50–70°N in the North Atlantic. The HOSING experiment is the same experiment as in Gu and Liu (2017). HOSING is initialized from the end of CTRL and is integrated for 1,400 model years, using the same $f_{boundary}$ and $\frac{[Nd]_p}{[Nd]_d}$ and the Coordinated Ocean-ice Reference Experiments, phase II, surface forcing as in CTRL.

3. Results

3.1. The Control Experiment

The results from the *p*-fixed and *p*-coupled Nd setups are virtually identical in CTRL. This is expected, as the particle fields used in the *p*-fixed Nd setup are the climatology of the particle fields in the *p*-coupled Nd setup under present-day climate forcing. Therefore, for the present-day CTRL simulation, the decadal mean Nd and ε_{Nd} results are the same in the *p*-fixed and *p*-coupled Nd setup. The discussion of Nd and ε_{Nd} in CTRL below will therefore not refer explicitly to *p*-fixed or *p*-coupled.

The Nd inventory in CTRL is 4.3×10^{12} g. This value is in agreement with the model-based estimates in Arsouze et al. (2009), Rempfer et al. (2011), and Tachikawa et al. (2003; 4.2×10^{12} g). The simulated

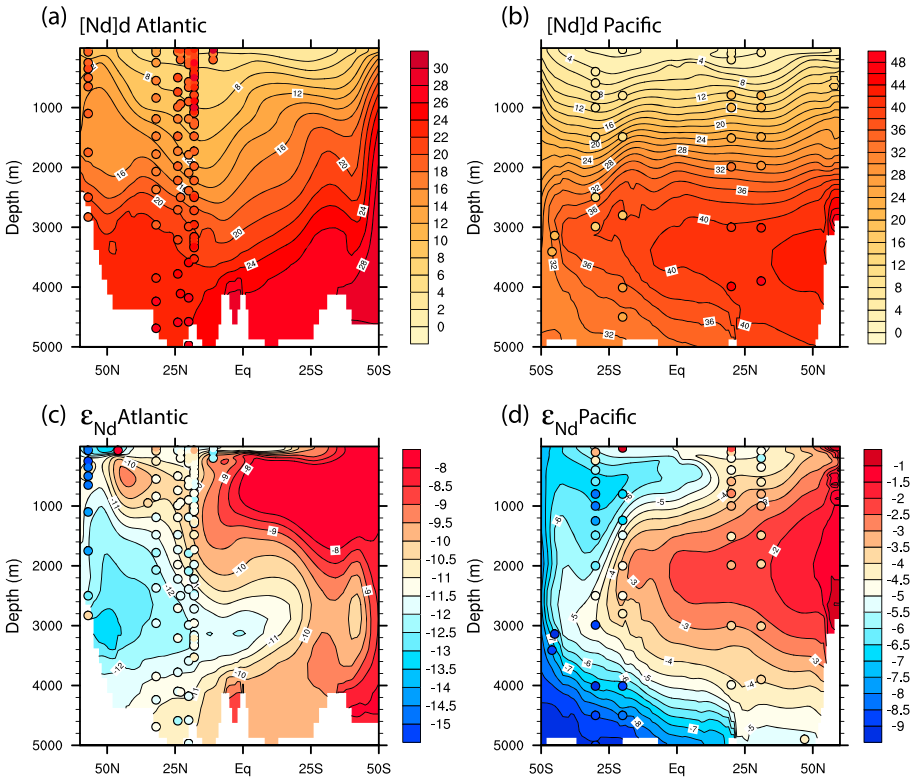

Figure 1. Nd concentration (a and b) and ε_{Nd} (c and d) in the vertical section in the Atlantic (20–30°W) and the Pacific (150–160°W) in CTRL. Observations (from the same regions) are superimposed as filled circles using the same color scale.

residence time of Nd is 785 years, which is comparable with previous modeling estimates of 700 years (Rempfer et al., 2011) and ~500 years (Siddall et al., 2008; Tachikawa et al., 2003) but is longer than the 360 years found in the modeling study of Arsouze et al. (2009). The much smaller residence time estimated in Arsouze et al. (2009) than in Rempfer et al. (2011) and in this study is mainly caused by differences in the magnitude of the global Nd sources. The residence time is calculated using the total Nd inventory divided by the total sources (dust source, river source, and boundary source). The estimated Nd inventory is similar in the different modeling studies (4.3×10^{12} to 4.2×10^{12} g), but the total source is 1.136×10^{10} g/year in Arsouze et al. (2009), 6.1×10^{9} g/year in Rempfer et al. (2011), and 5.51×10^{9} g/year in this study. Therefore, the estimated residence time in this study is similar to Rempfer et al. (2011) but is much larger than the estimate in Arsouze et al. (2009).

The general features of the Nd concentration distribution in CTRL are in reasonable agreement with the observations and are comparable with results from previous modeling studies. The Nd concentrations in CTRL increase with depth and along the circulation pathway from the North Atlantic to the North Pacific, which is in agreement with the observations (Figures 1 and 2). Figure 1 shows a vertical section in the Atlantic (20–30°W) and the Pacific (150–160°W) in CTRL with observations in this region overlaid. Figure 2 shows near-seafloor Nd concentrations in CTRL with several vertical profiles along with observations. The largest Nd concentrations are found in the abyssal North Pacific. As in the observations, the Nd concentrations generally increases with depth (Figures 1a and 1b and 2). However, the surface Nd concentrations in CTRL are generally smaller than in the observations, while the deep ocean concentrations are generally larger than in the observations, especially in the Pacific (Figure 4). Low Nd concentrations in the surface ocean compared to the observations were also found in previous Nd modeling studies (Arsouze et al., 2009; Rempfer et al., 2011), probably because of a similar modeling scheme applied in these studies. This indicates that the representation of the processes governing Nd concentrations in the ocean needs further improvements and should be a focus in future Nd modeling studies.

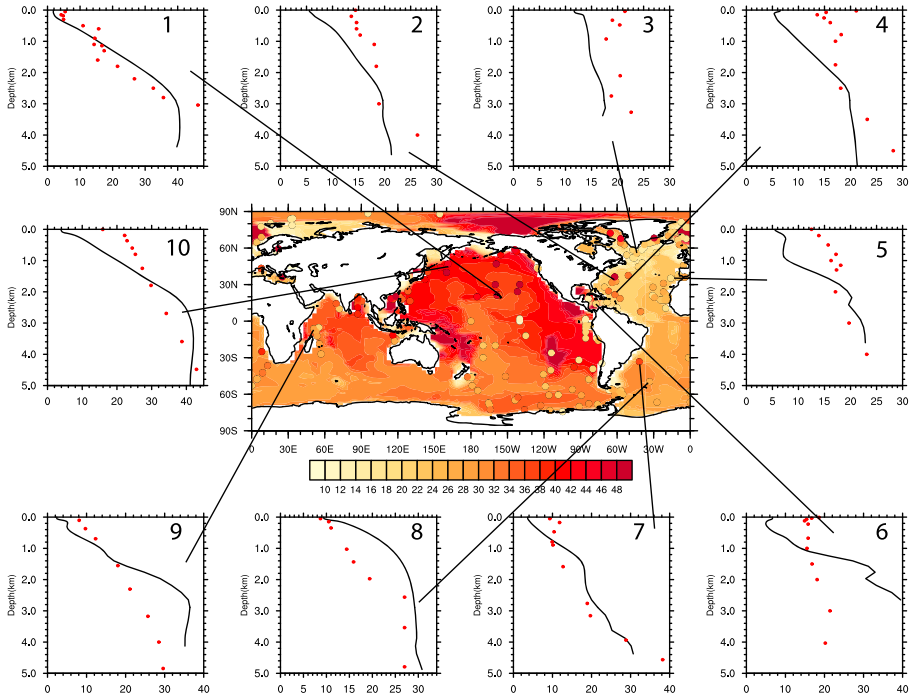

Figure 2. In shading, the seafloor Nd concentration in CTRL is shown. Observations are superimposed as filled circles using the same color scale. In profiles 1–10, selected vertical Nd concentration profiles are shown, using a black line for CTRL and red dots for observations.

The ε_{Nd} distribution in CTRL agrees well with the observations and shows distinct water mass properties (Figures 1c and 1d and 3). The vertical section of ε_{Nd} in the Atlantic shows a southward propagation of unradiogenic NADW and a northward movement of less unradiogenic AAIW and AABW (Figure 1c). In the Pacific, the distribution of ε_{Nd} shows a southward movement of radiogenic North Pacific Deep Water and a northward movement of AAIW and AABW (Figure 1d). Observations of ε_{Nd} near the seafloor show the most radiogenic waters in the North Pacific, while the most unradiogenic waters are found in the Labrador Sea. This interbasin gradient in ε_{Nd} is well reproduced in CTRL (Figure 3). Most simulated vertical profiles of ε_{Nd} reproduce the vertical distribution of ε_{Nd} in the observations (Figure 3), especially the "zigzag" pattern in the Atlantic (Goldstein & Hemming, 2003; Figure 3, profiles 2, 4, 5, and 7), which shows the vertically alternating water masses with depth, from AAIW to NADW and eventually to AABW. Our model also produces the observed radiogenic ε_{Nd} in the Caribbean Sea (Osborne et al., 2014; Figure 3, profile 6), which has been suggested to be important for interpreting ε_{Nd} reconstructions in the tropical Atlantic at intermediate depth (Gu et al., 2017). More quantitatively, linear regression coefficients are used to assess the model performance for ε_{Nd}. We find that ε_{Nd} is in better agreement with observations in the Atlantic and the Pacific than in the Indian Ocean (Table 2). In addition, in the Atlantic and the Pacific, ε_{Nd} is better simulated below 1,000 m than above 1,000 m (Table 2 and Figures 3 and 4). The largest deviations from observations are found in the upper 1,000 m (Figure 3 and Table 2). One potential cause of this surface bias is in the prescribed IR of the dust source and river source. Rempfer et al. (2011) showed that ε_{Nd} is substantially influenced by these surface sources in the upper 1,000 m but is controlled mainly by the boundary source below 1,000 m. Furthermore, the ε_{Nd} values in the surface are much more variable than in the deeper ocean (Goldstein & Hemming, 2003) both in the observations and in the model. Since most of the marine ε_{Nd} proxy data used for paleocirculation reconstructions are from samples taken at intermediate and deep depths, the model ε_{Nd} biases in the upper layers are unlikely to have a large impact on such paleoceanographic interpretations between the model and such observations. However, it should be noted that caution has to be used when applying our model to help interpret data in the upper ocean above 1,000 m.

The zonal mean ε_{Nd} in the Atlantic covaries with salinity in CTRL (Figure 5a), which is an indication of the ability of ε_{Nd} to trace different water masses (Goldstein & Hemming, 2003). However, compared with

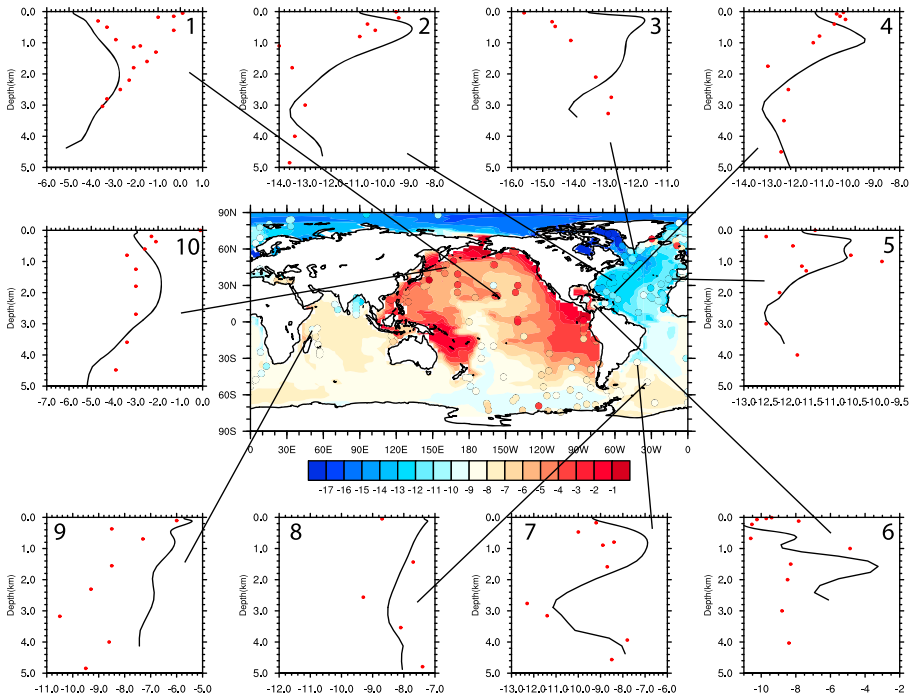

Figure 3. The seafloor ε_{Nd} in CTRL is shown as a shaded plot. Observations are superimposed as filled circles using the same color scale. In profiles 1–10, selected ε_{Nd} profiles are also shown, with a black line for CTRL and red dots for observations.

salinity, the NADW tongue represented by ε_{Nd} is shifted to a deeper depth. This is similar to the findings by Rempfer et al. (2011) and is attributed to the reversible scavenging that transports ε_{Nd} values downward. With the increase of $\frac{[Nd]_p}{[Nd]_d}$, which represents an increase in strength of reversible scavenging, the local maxima/minima of ε_{Nd} profiles are shifted to deeper depths (Figure 5b). This downward shift is stronger in the upper ocean than in the deep ocean because the particle fluxes, and therefore, the influence of the reversible scavenging are larger in the upper ocean.

3.2. ε_{Nd} in Idealized Hosing Experiment

In response to the 1-Sv freshwater flux in the North Atlantic in HOSING, the AMOC strength reduces from 16 Sv in CTRL (AMOC-on state) to 2 Sv (AMOC-off state; Figure 6a). We first discuss the *p*-fixed ε_{Nd} in HOSING, which is caused purely by the circulation change and will then return to the *p*-coupled ε_{Nd} in HOSING, which also includes effects from changes in the particle fluxes.

Compared with the AMOC-on state, the *p*-fixed ε_{Nd} in the Atlantic during the AMOC-off state shows less southward penetration of NADW and less northward penetration of AAIW (Figure 7b). This is also reflected in the reduced zigzag pattern in the vertical profile of ε_{Nd} in the Atlantic (Figure 8, green line). The difference

Table 2
The Linear Regression Coefficient (rc) Between Model ε_{Nd} and Observational ε_{Nd} in Different Ocean Basins at Different Depth Range: 0–200, 200–1,000, 1,000–3,000 m, and Depth Deeper Than 3,000 m

Depth Range (m)	Atlantic *N*	Atlantic rc	Pacific *N*	Pacific rc	Indian *N*	Indian rc
Total	851	0.54	668	0.56	180	0.23
0–200	250	0.43	177	0.32	41	0.38
200–1,000	264	0.47	196	0.47	82	0.16
1,000–3,000	254	0.75	207	0.97	45	0.29
>3,000	83	0.98	88	1.05	12	0.04

Note. *N* is the number of points. Linear regression coefficient tells the amount of model ε_{Nd} change can be expected from a unit increase of observational ε_{Nd}.

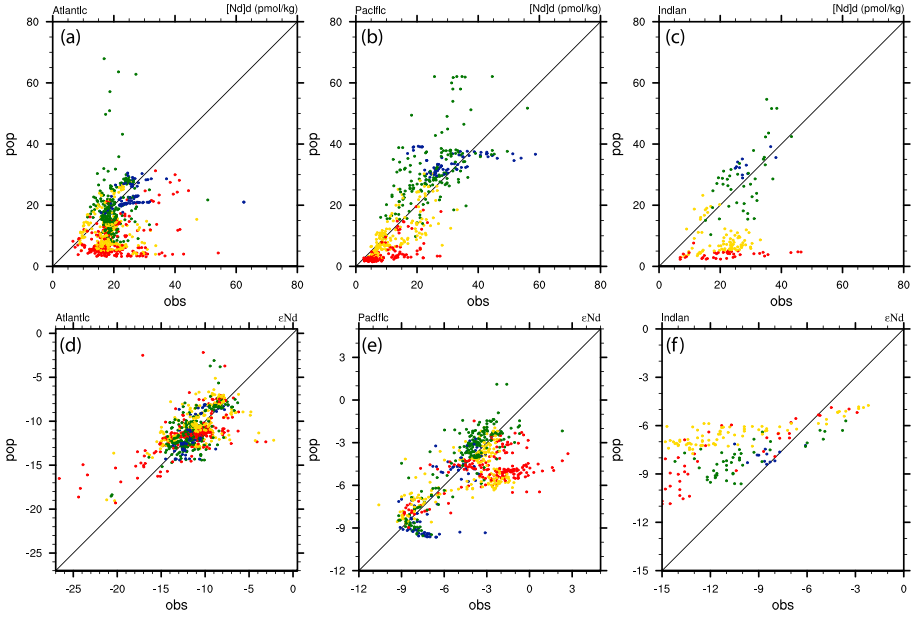

Figure 4. Scatter plot of Nd concentration (a–c) and ε_{Nd} (d–f) between observations (x axis) and CTRL (y axis) in different ocean basins. The Southern Ocean is included in the respective Atlantic Ocean, Pacific Ocean, and Indian Ocean sections. Observations in different depth ranges are indicated by different colors: 0–200 m (red), 200–1,000 m (yellow), 1,000–3,000 m (green), and below 3,000 m (navy).

of the p-fixed ε_{Nd} between the AMOC-off and the AMOC-on states is shown in Figure 7c. The pattern of changes resembles that in Rempfer et al. (2012a). In the upper 1,000 m, the maximum change toward more unradiogenic ε_{Nd} values (by about −4 ε_{Nd} unit) is located at the equator. With the reduced strength of the AMOC, less AAIW is transported to the equatorial Atlantic (Gu et al., 2017). Therefore, p-fixed ε_{Nd} in the equatorial Atlantic experiences an unradiogenic change (negative change). In the depth range of 1,000 to 3,000 m, the most radiogenic change (positive change; about +3 ε_{Nd} unit) is located at 30°S. The freshwater flux in the North Atlantic inhibits the formation of NADW, leading to less unradiogenic NADW transported to the South Atlantic. Therefore, p-fixed ε_{Nd} in the South Atlantic experiences a radiogenic shift. Below 4,000 m, AABW shows a radiogenic change (positive change; about +1 ε_{Nd} unit), which is much more uniform across different latitudes than in the upper ocean because there is little change in the strength of the lower cell of the AABW (Figures 7a and 7b).

The stability of ε_{Nd} end-members is important for the application of ε_{Nd} as a proxy for water mass mixing (e.g., Huang et al., 2014; Piotrowski et al., 2004). To evaluate the stability of ε_{Nd} end-member values in the

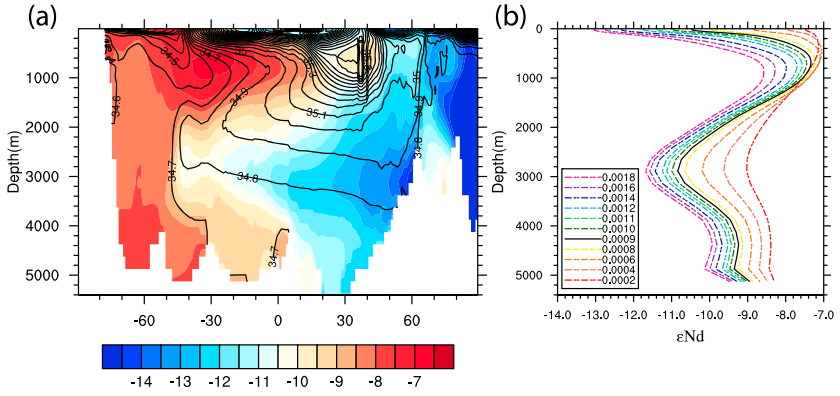

Figure 5. (a) Atlantic zonal mean p-fixed ε_{Nd} (color) and salinity (contour). (b) South Atlantic (0° to 30°S) mean p-fixed ε_{Nd} vertical profile in different experiments with varying $\frac{[Nd]_p}{[Nd]_d}$ ($f_{boundary} = 4 \times 10^9$ g/year).

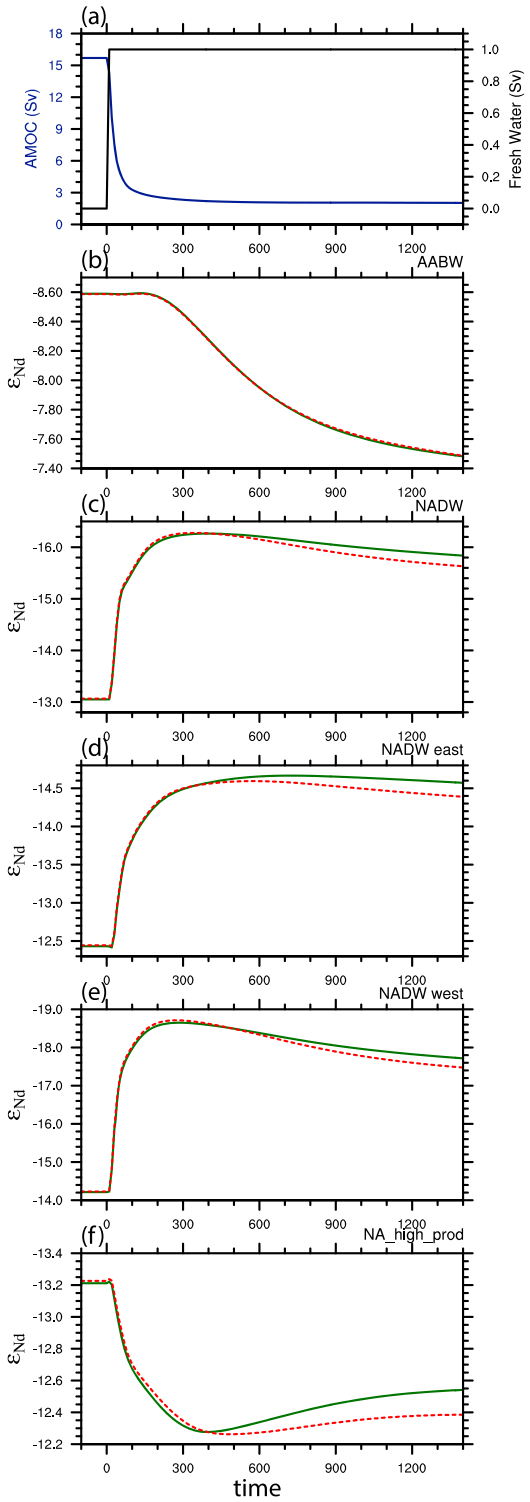

Figure 6. Time evolutions (decadal mean) in the HOSING experiment. (a) Freshwater forcing (black) and AMOC strength (navy). (b) The ε_{Nd} value for the AABW end-member, which is calculated as the average of 60–70°S below 4,000 m. (c) The ε_{Nd} value for the NADW end-member, which is calculated as the average of 50–60°N between 2,500 and 3,000 m. (d) The ε_{Nd} value for the NADW in the East Atlantic, which is calculated as the average of 50–60°N between 2,500 and 3,000 m east of 20°W. (e) The ε_{Nd} value for the NADW in the West Atlantic, which is calculated as the average of 50–60°N between 2,500 and 3,000 m west of 50°W. (f) The ε_{Nd} value at 2,890 m at (40°N, 40°W), where productivity experiences great changes in HOSING. In the ε_{Nd} time series (b–f), green is *p*-fixed ε_{Nd} and red is *p*-coupled ε_{Nd}. AMOC = Atlantic Meridional Overturning Circulation; AABW = Antarctic Bottom Water; NADW = North Atlantic Deep Water.

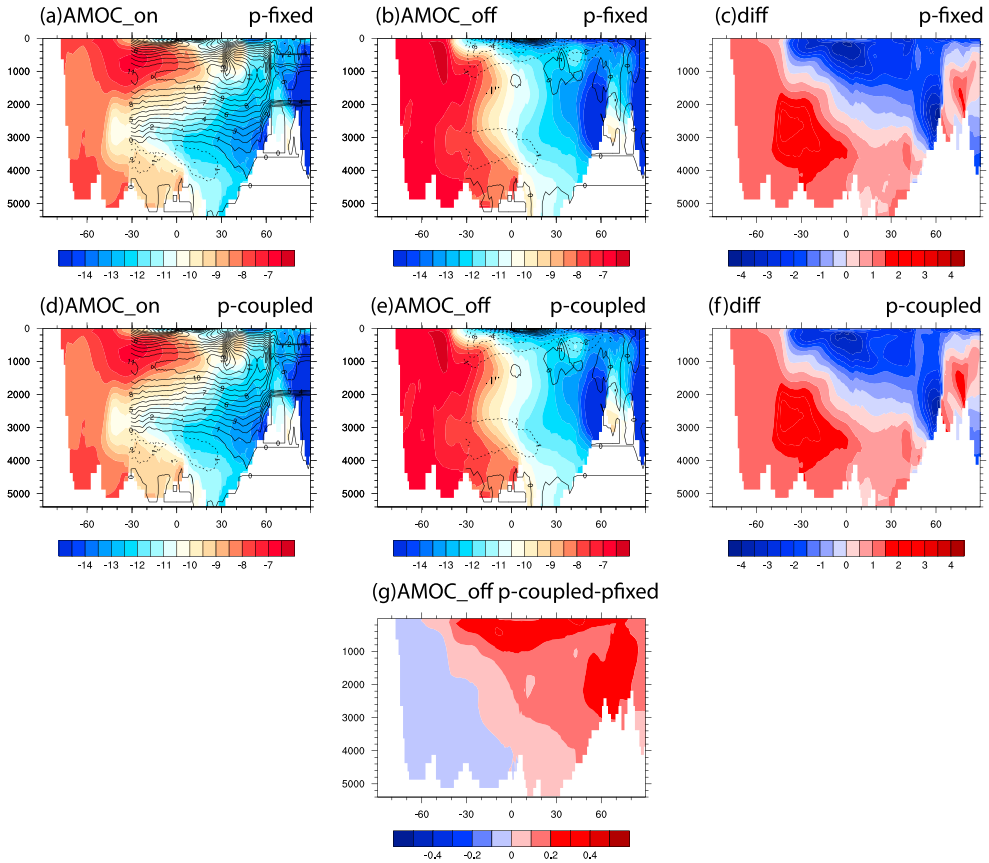

Figure 7. Atlantic zonal mean *p*-fixed ε_{Nd} (color) and the Atlantic meridional overturning stream function (contour) in the AMOC-on (a) and AMOC-off (b) states. The difference in Atlantic zonal mean *p*-fixed ε_{Nd} between AMOC-off and AMOC-on (c). (d–f) The same as (a)–(c) for *p*-coupled ε_{Nd}. In (g), the difference between *p*-coupled and *p*-fixed ε_{Nd} during AMOC-off is shown. AMOC = Atlantic Meridional Overturning Circulation.

idealized hosing experiment, we examine the ε_{Nd} end-member values in the AABW and NADW. It should be noted that in this study we only consider the influence of ocean circulation on the ε_{Nd} end-member values. Previous studies suggest that changes in the Nd sources or the bathymetry could also influence ε_{Nd} end-member values (Arsouze et al., 2008). However, sensitivity experiments in Rempfer et al. (2012b) suggest that substantial changes in Nd sources or ε_{Nd} are required to generate ε_{Nd} changes in the deep ocean that have a magnitude comparable to the ε_{Nd} reconstructed changes for glacial-interglacial scales.

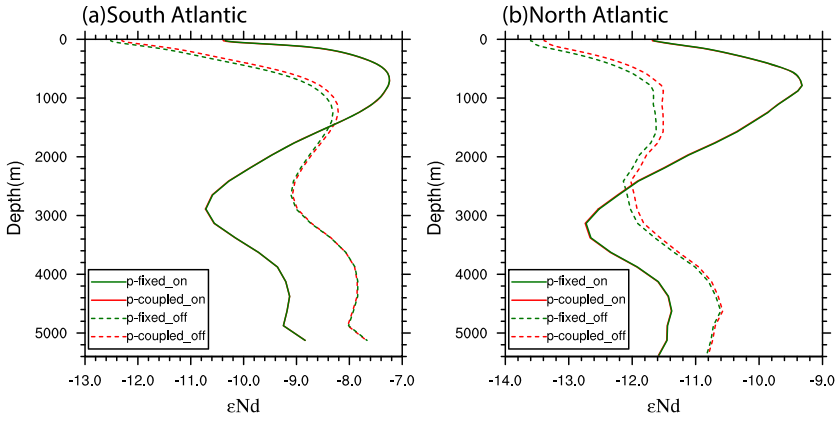

Figure 8. South Atlantic (a) and North Atlantic (b) mean ε_{Nd} profiles during AMOC-on (solid line) and AMOC-off (dash line) states for *p*-fixed (green) and *p*-coupled (red) ε_{Nd}. AMOC = Atlantic Meridional Overturning Circulation.

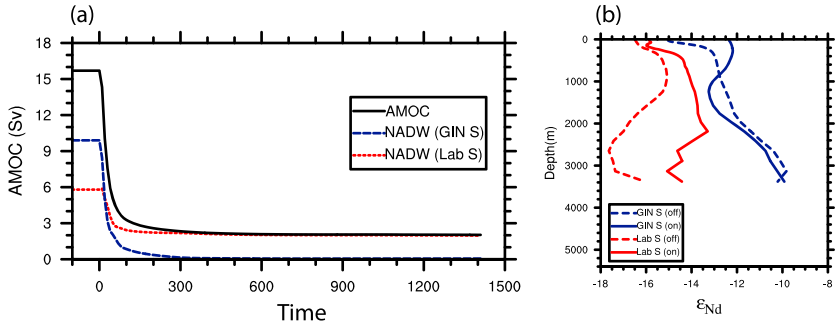

Figure 9. (a) AMOC strength (solid black) and deepwater formation rate in the Labrador Sea (Lab S) region (dash red) and the GIN Sea (GIN S) region (dash navy). Deepwater formation rate in the GIN Sea is defined as the maximum of the stream function at 62°N. Deepwater formation rate in the Labrador Sea is defined as the difference between the AMOC strength and the deepwater formation rate in the GIN Sea. (b) The vertical profiles of ε_{Nd} in the Labrador Sea (red) and the GIN Sea (navy) during the AMOC_on state (solid) and the AMOC_off state (navy). AMOC = Atlantic Meridional Overturning Circulation; NADW = North Atlantic Deep Water.

In HOSING, the AABW end-member experiences a radiogenic change. The end-member value of AABW is calculated as the average ε_{Nd} from 60°S to 70°S below 4000 m in the Southern Ocean. The AABW end-member ε_{Nd} value shifts from −8.6 in AMOC-on to −7.5 in AMOC-off (Figure 6b). The ε_{Nd} of the water from circum-Antarctica derives its value from the mixing of the radiogenic Pacific waters and the unradiogenic NADW (Goldstein & Hemming, 2003; von Blanckenburg, 1999). During the AMOC-off state, less NADW is transported from the North Atlantic to the Southern Ocean, which leads to a radiogenic shift in the AABW end-member value. The uniform 1 ε_{Nd} unit radiogenic change in the abyssal Atlantic (Figure 7c) is mainly due to the radiogenic change in the AABW end-member value.

The NADW end-member shows an unradiogenic (negative) shift in HOSING. The NADW end-member value is calculated as the average ε_{Nd} from 50°N to 60°N in the Atlantic between 2,500 and 3,000 m (Figure 6c). The NADW end-member value shows a 2.8 ε_{Nd} unit unradiogenic shift from the AMOC-on state to the AMOC-off state. NADW in the western North Atlantic (west of 50°W) is more unradiogenic and has a larger magnitude of change than in the eastern North Atlantic (east of 20°W; Figures 6d and 6e). NADW is formed in both the Labrador Sea and the GIN Sea. Water from the Labrador Sea in the western North Atlantic has the most unradiogenic ε_{Nd} and water from the GIN Sea is more radiogenic than the Labrador Sea (Figure 9b) because of the radiogenic input around Iceland (Figure S3). In HOSING, both the deepwater formation in the Labrador Sea and the GIN Sea are reduced, with almost no deepwater formation in the GIN Sea and about half of the initial formation in the Labrador Sea during the AMOC-off state. In the GIN Sea, the ε_{Nd} does not change much from the AMOC_on state to the AMOC_off state (Figure 9b). However, ε_{Nd} in the Labrador Sea shows a large unradiogenic shift from the surface to the bottom (Figure 9b). In the AMOC_off state, circulation in the subpolar region is greatly reduced. The Labrador Sea becomes more isolated and water in the Labrador Sea experiences reduced mixing with more radiogenic water from eastern North Atlantic. Hence, ε_{Nd} in the Labrador Sea becomes more unradiogenic (Figure S5). Therefore, the unradiogenic NADW end-member change in HOSING is due to the unradiogenic shift in the deepwater from the Labrador Sea and the missing contribution of more radiogenic waters from the GIN Sea.

The ε_{Nd} experiences opposite changes between the western and the eastern Atlantic south of 50°N (Figure 10). At 2,500 m, an unradiogenic shift starts from the east of Greenland at 60°N (Figure 10b) and expands into the entire North Atlantic from 50°N to 60°N and eventually to the eastern Atlantic south of 50°N (Figures 10c–10f). In the western Atlantic, the radiogenic shift occurs because of the reduced transport of water with unradiogenic ε_{Nd} from the high-latitude North Atlantic in the weakened western boundary current. In the eastern Atlantic, the unradiogenic shift is caused by the unradiogenic shift in the NADW endmember. Therefore, the effect of the NADW end-member change on ε_{Nd} in the Atlantic depends on the location. For example, during the AMOC-off state, the north-south gradient of ε_{Nd} in the Atlantic becomes even greater than in the AMOC-on state. The radiogenic ε_{Nd} shift from 2,000 to 3,000 m in the South Atlantic (Figure 7c) cannot be attributed to the unradiogenic change in the NADW end-member value because of the opposite direction of the changes; instead, this radiogenic change in the South Atlantic is

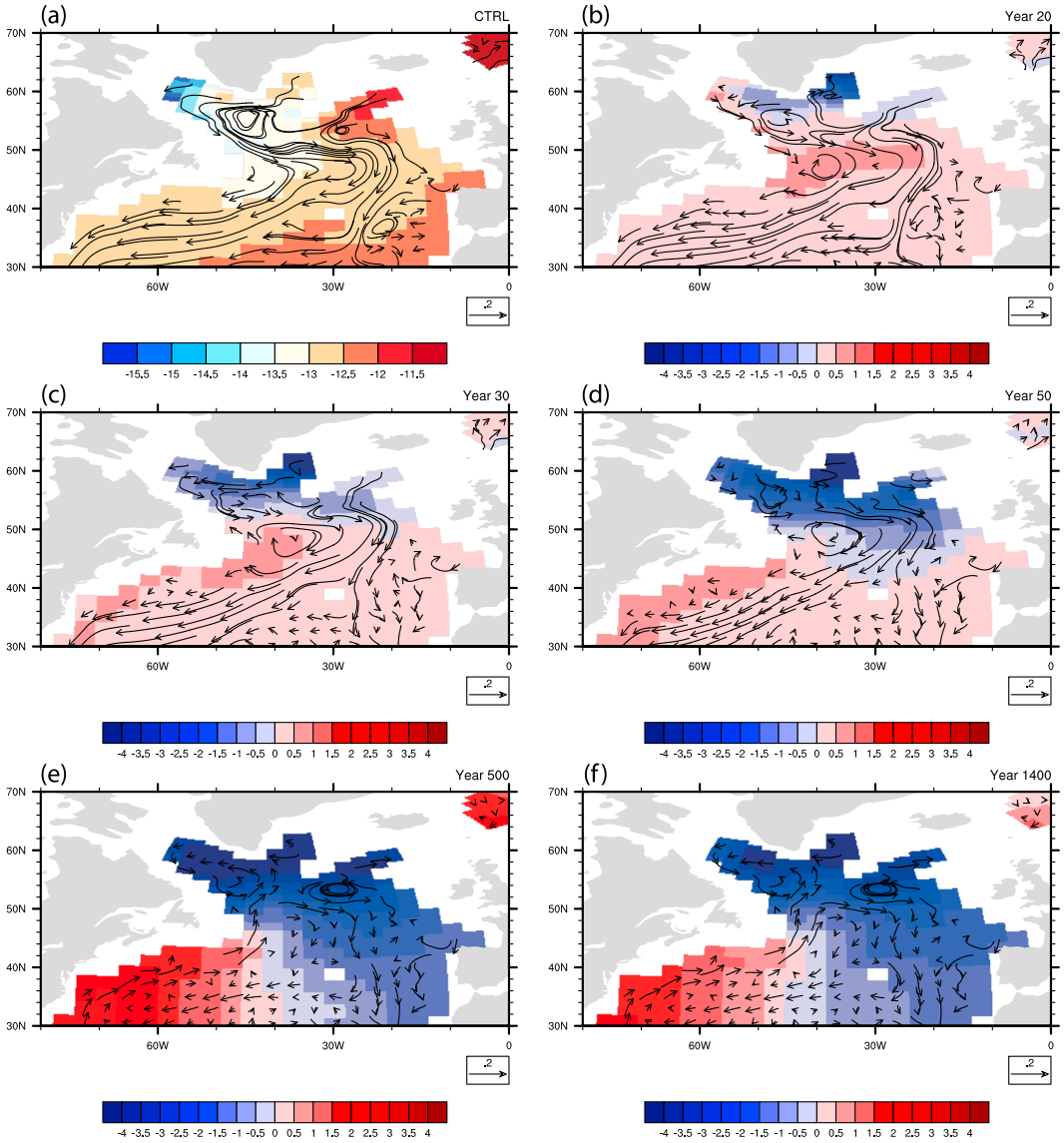

Figure 10. The ε_{Nd} (p-fixed) at 2,500 m in CTRL (a) and the difference between different times in HOSING and CTRL (b–f). Velocity (cm/s) at different times is overlaid in each plot.

mainly caused by the reduced southward transport of NADW. However, the unradiogenic change of ε_{Nd} in the North Atlantic at 2,500 m (Figure 10f) can be explained, at least in part, by the NADW end-member change. Hence, our results show that changes in the end-member ε_{Nd} values may be important when interpreting ε_{Nd} reconstructions, depending on the location of sites.

Comparing the HOSING run in the CESM with the hosing experiment in the Bern3D model (Rempfer et al., 2012a), a common feature is that the largest changes are simulated in the equatorial Atlantic at intermediate depth and in the deep South Atlantic. However, the response of the two models is different in the North Atlantic in the deep ocean (2,000–3,000 m). From the AMOC-on state to the AMOC-off state, the unradiogenic shift in the high latitude North Atlantic (60°N) expands to the whole North Atlantic from the eastern Atlantic in CESM (Figures 7c and 10). In Rempfer et al. (2012a), the high latitude North Atlantic also experiences an unradiogenic shift from AMOC-on to AMOC-off, but it is confined to north of 50°N. This difference may be caused by the lower model resolution and simplified model dynamics in Rempfer et al. (2012a) compared to the CESM used here.

In HOSING, the productivity of $CaCO_3$, opal, and POC in the North Atlantic is greatly reduced (Gu & Liu, 2017) because of reduced nutrient supply resulting from the increase of stratification (Plattner et al., 2001; Schmittner, 2005). The resulting particle flux changes could also lead to a change in the *p*-coupled ε_{Nd} (Rempfer et al., 2011). However, by comparing results from the *p*-coupled and *p*-fixed Nd setups, we find that the ε_{Nd} changes in our model are mainly controlled by the circulation change. This is different from $^{231}Pa/^{230}Th$ in the CESM, which was found to be controlled by both the circulation and the productivity of biogenic particles (Gu & Liu, 2017). The changes in ε_{Nd} caused by changes in biological productivity are much smaller than the ε_{Nd} changes caused by changes in the circulation (Figures 7c, 7f, and 7g). The *p*-coupled ε_{Nd} shows almost identical changes to the *p*-fixed ε_{Nd} (Figures 6–8). For example, at a site at 40°N and 40°W (Figure 6f), where the productivity of opal and POC experiences large changes and the $^{231}Pa/^{230}Th$ response in HOSING differs significantly between the two setups (Gu & Liu, 2017), the ε_{Nd} difference between *p*-fixed and *p*-coupled is rather small compared with the ε_{Nd} changes due to the circulation change alone. The different impact of the particle flux changes on ε_{Nd} and $^{231}Pa/^{230}Th$ is that the partition coefficients (K) are the same for ^{143}Nd and ^{144}Nd due to their near-identical chemical properties and their similar molecular mass. Therefore, there is no differentiation between ^{143}Nd and ^{144}Nd by reversible scavenging. In contrast, K values are different for ^{231}Pa and ^{230}Th, two different chemical elements, which leads to different scavenging rates between ^{231}Pa and ^{230}Th and changes in the particle fluxes will cause changes in the $^{231}Pa/^{230}Th$ distribution. The small difference between *p*-fixed and *p*-coupled ε_{Nd} in HOSING indicates that the effect of particle flux changes on the ε_{Nd} distribution is likely secondary compared with the effect of circulation change caused by freshwater forcing. This is consistent with the findings in Rempfer et al. (2012a) and hence shows that this result holds in a more complex ocean model.

4. Discussion and Conclusion

In this study, we described the implementation of Nd isotopes into the CESM1.3 ocean component and evaluated the overall model performance in simulating the marine Nd cycle. One of the major objectives was to document the Nd implementation for future community references. Our implementation largely follows previous works (Arsouze et al., 2009; Rempfer et al., 2011; Siddall et al., 2008). Nd isotopes were implemented in CESM1 using both *p*-fixed and *p*-coupled versions, working without and with an active biogeochemical module, respectively. We showed that overall, our model is able to reproduce the major features of the observed distributions of the Nd concentration and ε_{Nd} under present-day climate forcing: the Nd concentration shows a nutrient-like distribution, increasing with depth and along the circulation pathway; ε_{Nd} traces different water masses.

Another major objective of this study was to examine the effect of changing NADW formation on ε_{Nd} in the Atlantic and ε_{Nd} end-member values, in a comprehensive ocean model. In our idealized hosing experiment, ε_{Nd} in the Atlantic shows the expected effect of circulation changes on the ε_{Nd} distribution. With a reduced AMOC strength, the simulated ε_{Nd} distribution shows a retreat of the northward propagating AAIW and southward propagating NADW. The AABW end-member value shows a radiogenic shift under reduced AMOC because of less unradiogenic input from the North Atlantic, which leads to a uniform 1-unit radiogenic ε_{Nd} change in the abyssal Atlantic. The NADW end-member value shows an unradiogenic shift, which leads to the nonuniform ε_{Nd} changes between the eastern and western North Atlantic south of 50°N and in the depth range of the NADW. Therefore, our idealized hosing experiment suggests that the influence of the ε_{Nd} end-member change on the interpretation of ε_{Nd} in the Atlantic depends on the location and should be treated with caution.

In response to the freshwater forcing in the North Atlantic, particle fluxes are changed substantially. However, the *p*-fixed and *p*-coupled ε_{Nd} shows very similar changes. This suggests that, in response to freshwater forcing, ε_{Nd} appears to be mainly influenced by the changes in the water mass mixing and circulation, while the effect of particle flux change on ε_{Nd} distribution is negligible. This result confirms the finding of Rempfer et al. (2012a) that the effect of the changes in the particle fluxes on ε_{Nd} is much smaller compared with the effect of the changes in the ocean circulation. This means that the computationally more efficient *p*-fixed version (without an active ocean BGC model) can be used to capture first-order effects in ε_{Nd} in modeling studies.

The implementation of Nd in CESM1 further enhances the power of the model as a tool for paleoclimate research. In particular, the same ocean component in the CESM1 has many other tracers, notably, $\delta^{18}O$ (Zhang et al., 2017), $^{231}Pa/^{230}Th$ (Gu & Liu, 2017), and $\delta^{13}C$ and radiocarbon (Jahn et al., 2015). The now also Nd-enabled CESM provides a powerful tool for the research community to improve the understanding of past ocean circulation changes in the future.

Acknowledgments
This work is supported by U.S. National Science Foundation (NSF) P2C2 projects (1401778, 1401802, and 1566432), Department of Energy (DOE) project DE-SC0006744, and the National Science Foundation of China 41630527. F. J. thanks for the support by the Swiss National Science Foundation (200020_172476) and the Swiss National Supercomputing Centre CSCS. J. Z. is supported by the DOE Regional and Global Climate Modeling program through support of the HiLAT project and the Center for Nonlinear Studies sponsored by Laboratory Directed Research and Development at Los Alamos National Laboratory. Computing resources (ark:/85065/d7wd3xhc) were provided by the Climate Simulation Laboratory at NCAR's Computational and Information Systems Laboratory, sponsored by the NSF and other agencies. Data used to produce the results can be obtained from HPSS at CISL: /home/sgu28/ND_implementation or by contacting the authors. Access to the NCAR HPSS can be freely obtained by anyone (https://www2.cisl.ucar.edu/resources/storage-and-file-systems/hpss/access). The code for simulating Nd in the CESM1 is stored here: https://zenodo.org/record/1468108#.XDR9wc8zYxg website. This code works with CESM version 1.3.

References

Amakawa, H., Sasaki, K., & Ebihara, M. (2009). Nd isotopic composition in the central North Pacific. *Geochimica et Cosmochimica Acta*, *73*(16), 4705–4719. https://doi.org/10.1016/j.gca.2009.05.058

Arsouze, T., Dutay, J.-C., Kageyama, M., Lacan, F., Alkama, R., Marti, O., & Jeandel, C. (2008). A modeling sensitivity study of the influence of the Atlantic meridional overturning circulation on neodymium isotopic composition at the Last Glacial Maximum. *Climate of the Past*, *4*(3), 191–203. https://doi.org/10.5194/cp-4-191-2008

Arsouze, T., Dutay, J. C., Lacan, F., & Jeandel, C. (2007). Modeling the neodymium isotopic composition with a global ocean circulation model. *Chemical Geology*, *239*(1–2), 165–177. https://doi.org/10.1016/j.chemgeo.2006.12.006

Arsouze, T., Dutay, J. C., Lacan, F., & Jeandel, C. (2009). Reconstructing the Nd oceanic cycle using a coupled dynamical- biogeochemical model. *Biogeosciences*, *6*(12), 2829–2846. https://doi.org/10.5194/bg-6-2829-2009

Bacon, M., & Anderson, R. (1982). Distribution of thorium isotopes between dissolved and particulate forms in the deep sea. *Journal of Geophysical Research*, *87*(C3), 2045–2056. https://doi.org/10.1029/JC087iC03p02045

Bertram, C. J., & Elderfield, H. (1993). The geochemical balance of the rare earth elements and neodymium isotopes in the oceans. *Geochimica et Cosmochimica Acta*, *57*(9), 1957–1986. https://doi.org/10.1016/0016-7037(93)90087-D

Crocket, K. C., Vance, D., Gutjahr, M., Foster, G. L., & Richards, D. A. (2011). Persistent Nordic deep-water overflow to the glacial North Atlantic. *Geology*, *39*(6), 515–518. https://doi.org/10.1130/G31677.1

Danabasoglu, G., Bates, S. C., Briegleb, B. P., Jayne, S. R., Jochum, M., Large, W. G., et al. (2012). The CCSM4 ocean component. *Journal of Climate*, *25*(5), 1361–1389. https://doi.org/10.1175/JCLI-D-11-00091.1

Deng, F., Thomas, A. L., Rijkenberg, M. J. A., & Henderson, G. M. (2014). Controls on seawater ^{231}Pa, ^{230}Th and ^{232}Th concentrations along the flow paths of deep waters in the Southwest Atlantic. *Earth and Planetary Science Letters*, *390*, 93–102. https://doi.org/10.1016/j.epsl.2013.12.038

Dokken, T. M., & Jansen, E. (1999). Rapid changes in the mechanism of ocean convection during the last glacial period. *Nature*, *401*(6752), 458–461. https://doi.org/10.1038/46753

Dutay, J.-C., Lacan, F., Roy-Barman, M., & Bopp, L. (2009). Influence of particle size and type on ^{231}Pa and ^{230}Th simulation with a global coupled biogeochemical-ocean general circulation model: A first approach. *Geochemistry, Geophysics, Geosystems*, *10*, Q01011. https://doi.org/10.1029/2008GC002291

Goldstein, S. L., & Hemming, S. R. (2003). Long-lived isotopic tracers in oceanography, paleoceanography, and ice-sheet dynamics. *Treatise on Geochemistry*, *6*(6), 453–489.

Goldstein, S. L., & Jacobsen, S. B. (1987). The Nd and Sr isotopic systematics of river-water dissolved material: Implications for the sources of Nd and Sr in seawater. *Chemical Geology: Isotope Geoscience Section*, *66*(3–4), 245–272.

Goldstein, S. L., O'Nions, R. K., & Hamilton, P. J. (1984). A Sm-Nd isotopic study of atmospheric dusts and particulates from major river systems. *Earth and Planetary Science Letters*, *70*(2), 221–236. https://doi.org/10.1016/0012-821X(84)90007-4

Greaves, M., Statham, P., & Elderfield, H. (1994). Rare earth element mobilization from marine atmospheric dust into seawater. *Marine Chemistry*, *46*(3), 255–260. https://doi.org/10.1016/0304-4203(94)90081-7

Grousset, F. E., Biscaye, P. E., Zindler, a., Prospero, J., & Chester, R. (1988). Neodymium isotopes as tracers in marine sediments and aerosols: North Atlantic. *Earth and Planetary Science Letters*, *87*(4), 367–378. https://doi.org/10.1016/0012-821X(88)90001-5

Grousset, F. E., Parra, M., Bory, A., Martinez, P., Bertrand, P., Shimmield, G., & Ellam, R. M. (1998). Saharan wind regimes traced by the Sr-Nd isotopic composition of subtropical Atlantic sediments: Last Glacial Maximum vs Today. *Quaternary Science Reviews*, *17*(4–5), 395–409. https://doi.org/10.1016/S0277-3791(97)00048-6

Gu, S., & Liu, Z. (2017). 231Pa and 230Th in the ocean model of the Community Earth System Model (CESM1. 3). *Geoscientific Model Development*, *10*(12), 4723–4742. Retrieved from https://doi.org/10.5194/gmd-10-4723-2017

Gu, S., Liu, Z., Zhang, J., Rempfer, J., Joos, F., & Oppo, D. W. (2017). Coherent response of Antarctic Intermediate Water and Atlantic Meridional Overturning Circulation during the last deglaciation: Reconciling contrasting neodymium isotope reconstructions from the tropical Atlantic. *Paleoceanography*, *32*, 1036–1053. https://doi.org/10.1002/2017PA003092

Hayes, C. T., Anderson, R. F., Fleisher, M. Q., Vivancos, S. M., Lam, P. J., Ohnemus, D. C., et al. (2015). Intensity of Th and Pa scavenging partitioned by particle chemistry in the North Atlantic Ocean. *Marine Chemistry*, *170*, 49–60. https://doi.org/10.1016/j.marchem.2015.01.006

Henderson, G. M., Heinze, C., Anderson, R. F., & Winguth, A. M. E. (1999). Global distribution of the ^{230}Th flux to ocean sediments constrained by GCM modelling. *Deep-Sea Research Part I: Oceanographic Research Papers*, *46*(11), 1861–1893. https://doi.org/10.1016/S0967-0637(99)00030-8

Howe, J. N. W., Piotrowski, A. M., & Rennie, V. C. F. (2016). Abyssal origin for the early Holocene pulse of unradiogenic neodymium isotopes in Atlantic seawater. *Geology*, *44*(10), 831–834. https://doi.org/10.1130/G38155.1

Huang, K.-F., Oppo, D. W., & Curry, W. B. (2014). Decreased influence of Antarctic intermediate water in the tropical Atlantic during North Atlantic cold events. *Earth and Planetary Science Letters*, *389*, 200–208. https://doi.org/10.1016/j.epsl.2013.12.037

Hurrell, J. W., Holland, M. M., Gent, P. R., Ghan, S., Kay, J. E., Kushner, P. J., et al. (2013). The community earth system model: A framework for collaborative research. *Bulletin of the American Meteorological Society*, *94*(9), 1339–1360. https://doi.org/10.1175/BAMS-D-12-00121.1

Jacobsen, S. B., & Wasserburg, G. J. (1980). Sm-Nd isotopic evolution of chondrites. *Earth and Planetary Science Letters*, *50*(1), 139–155. https://doi.org/10.1016/0012-821X(80)90125-9

Jahn, A., Lindsay, K., Giraud, X., Gruber, N., Otto-Bliesner, B. L., Liu, Z., & Brady, E. C. (2015). Carbon isotopes in the ocean model of the Community Earth System Model (CESM1). *Geoscientific Model Development*, *8*(8), 2419–2434. https://doi.org/10.5194/gmd-8-2419-2015

Jeandel, C. (1993). Concentration and isotopic composition of Nd in the South Atlantic Ocean. *Earth and Planetary Science Letters*, *117*(3-4), 581–591. Retrieved from http://www.sciencedirect.com/science/article/pii/0012821X9390104H, https://doi.org/10.1016/0012-821X(93)90104-H

Jeandel, C., Arsouze, T., Lacan, F., Techine, P., & Dutay, J. (2007). Isotopic Nd compositions and concentrations of the lithogenic inputs into the ocean: A compilation, with an emphasis on the margins. *Chemical Geology*, *239*(1–2), 156–164. https://doi.org/10.1016/j.chemgeo.2006.11.013

Jones, K. M., Khatiwala, S. P., Goldstein, S. L., Hemming, S. R., & van de Flierdt, T. (2008). Modeling the distribution of Nd isotopes in the oceans using an ocean general circulation model. *Earth and Planetary Science Letters*, *272*(3–4), 610–619. https://doi.org/10.1016/j.epsl.2008.05.027

Kriest, I. (2002). Different parameterizations of marine snow in a 1D-model and their influence on representation of marine snow, nitrogen budget and sedimentation. *Deep-Sea Research Part I: Oceanographic Research Papers*, *49*(12), 2133–2162. https://doi.org/10.1016/S0967-0637(02)00127-9

Labeyrie, L. D., Duplessy, J., Duprat, J., Juillet-Leclerc, A., Moyes, J., Michel, E., et al. (1992). Changes in the vertical structure of the North Atlantic Ocean between glacial and modern times. *Quaternary Science Reviews*, *11*(4), 401–413. https://doi.org/10.1016/0277-3791(92)90022-Z

Lacan, F., Tachikawa, K., & Jeandel, C. (2012). Neodymium isotopic composition of the oceans: A compilation of seawater data. *Chemical Geology*, *300-301*, 177–184. https://doi.org/10.1016/j.chemgeo.2012.01.019

Large, W. G., & Yeager, S. G. (2008). The global climatology of an interannually varying air–sea flux data set. *Climate Dynamics*, *33*(2–3), 341–364. https://doi.org/10.1007/s00382-008-0441-3

Luo, C., Mahowald, N., & Corral, J. (2003). Sensitivity study of meteorological parameters on mineral aerosol mobilization, transport, and distribution. *Journal of Geophysical Research*, *108*(D15), 4447. https://doi.org/10.1029/2003JD003483

Osborne, A. H., Haley, B. A., Hathorne, E. C., Flögel, S., & Frank, M. (2014). Neodymium isotopes and concentrations in Caribbean seawater: Tracing water mass mixing and continental input in a semi-enclosed ocean basin. *Earth and Planetary Science Letters*, *406*, 174–186. https://doi.org/10.1016/j.epsl.2014.09.011

Pahnke, K., Goldstein, S. L., & Hemming, S. R. (2008). Abrupt changes in Antarctic Intermediate Water circulation over the past. *Nature Geoscience*, *1*(12), 870–874. https://doi.org/10.1038/ngeo360

Piepgras, D., & Wasserburg, G. (1987). Rare earth element transport in the western North Atlantic inferred from Nd isotopic observations. *Geochimica et Cosmochimica Acta*, *51*(5), 1257–1271. https://doi.org/10.1016/0016-7037(87)90217-1

Piotrowski, A. M., Galy, A., Nicholl, J. A. L., Roberts, N., Wilson, D. J., Clegg, J. A., & Yu, J. (2012). Reconstructing deglacial North and South Atlantic deep water sourcing using foraminiferal Nd isotopes. *Earth and Planetary Science Letters*, *357-358*, 289–297. https://doi.org/10.1016/j.epsl.2012.09.036

Piotrowski, A. M., Goldstein, S. L., Hemming, S. R., & Fairbanks, R. G. (2004). Intensification and variability of ocean thermohaline circulation through the last deglaciation. *Earth and Planetary Science Letters*, *225*(1–2), 205–220. https://doi.org/10.1016/j.epsl.2004.06.002

Plattner, G. K., Joos, F., Stocker, T. F., & Marchal, O. (2001). Feedback mechanisms and sensitivities of ocean carbon uptake under global warming. *Tellus, Series B: Chemical and Physical Meteorology*, *53*(5), 564–592. https://doi.org/10.3402/tellusb.v53i5.16637

Rempfer, J., Stocker, T. F., Joos, F., & Dutay, J.-C. (2012a). On the relationship between Nd isotopic composition and ocean overturning circulation in idealized freshwater discharge events. *Paleoceanography*, *27*, PA3211. https://doi.org/10.1029/2012PA002312

Rempfer, J., Stocker, T. F., Joos, F., & Dutay, J.-C. (2012b). Sensitivity of Nd isotopic composition in seawater to changes in Nd sources and paleoceanographic implications. *Journal of Geophysical Research*, *117*, C12010. https://doi.org/10.1029/2012JC008161

Rempfer, J., Stocker, T. F., Joos, F., Dutay, J.-C., & Siddall, M. (2011). Modelling Nd-isotopes with a coarse resolution ocean circulation model: Sensitivities to model parameters and source/sink distributions. *Geochimica et Cosmochimica Acta*, *75*(20), 5927–5950. https://doi.org/10.1016/j.gca.2011.07.044

Rempfer, J., Stocker, T. F., Joos, F., Lippold, J., & Jaccard, S. L. (2017). New insights into cycling of ^{231}Pa and ^{230}Th in the Atlantic Ocean. *Earth and Planetary Science Letters*, *468*, 27–37. https://doi.org/10.1016/j.epsl.2017.03.027

Roberts, N. L., Piotrowski, A. M., McManus, J. F., & Keigwin, L. D. (2010). Synchronous deglacial overturning and water mass source changes. *Science*, *327*(5961), 75–78. https://doi.org/10.1126/science.1178068

Rousseau, T. C. C., Sonke, J. E., Chmeleff, J., van Beek, P., Souhaut, M., Boaventura, G., et al. (2015). Rapid neodymium release to marine waters from lithogenic sediments in the Amazon estuary. *Nature Communications*, *6*(1), 7592. https://doi.org/10.1038/ncomms8592

Schmittner, A. (2005). Decline of the marine ecosystem caused by a reduction in the Atlantic overturning circulation. *Nature*, *434*(7033), 628–633. https://doi.org/10.1038/nature03476

Siddall, M., Henderson, G. M., Edwards, N. R., Frank, M., Müller, S. a., Stocker, T. F., & Joos, F. (2005). ^{231}Pa/^{230}Th fractionation by ocean transport, biogenic particle flux and particle type. *Earth and Planetary Science Letters*, *237*(1–2), 135–155. https://doi.org/10.1016/j.epsl.2005.05.031

Siddall, M., Khatiwala, S., van de Flierdt, T., Jones, K., Goldstein, S. L., Hemming, S., & Anderson, R. F. (2008). Towards explaining the Nd paradox using reversible scavenging in an ocean general circulation model. *Earth and Planetary Science Letters*, *274*(3–4), 448–461. https://doi.org/10.1016/j.epsl.2008.07.044

Stichel, T., Frank, M., Rickli, J., & Haley, B. a. (2012). The hafnium and neodymium isotope composition of seawater in the Atlantic sector of the Southern Ocean. *Earth and Planetary Science Letters*, *317-318*, 282–294. https://doi.org/10.1016/j.epsl.2011.11.025

Tachikawa, K., Athias, V., & Jeandel, C. (2003). Neodymium budget in the modern ocean and paleo-oceanographic implications. *Journal of Geophysical Research*, *108*(C8), 3254. https://doi.org/10.1029/1999JC000285

van de Flierdt, T., Frank, M., Lee, D. C., Halliday, A. N., Reynolds, B. C., & Hein, J. R. (2004). New constraints on the sources and behavior of neodymium and hafnium in seawater from Pacific Ocean ferromanganese crusts. *Geochimica et Cosmochimica Acta*, *68*(19), 3827–3843. https://doi.org/10.1016/j.gca.2004.03.009

van de Flierdt, T., Griffiths, A. M., Lambelet, M., Little, S. H., Stichel, T., & Wilson, D. J. (2016). Neodymium in the oceans: A global database, a regional comparison and implications for palaeoceanographic research. *Philosophical Transactions of the Royal Society A: Mathematical, Physical and Engineering Sciences*, *374*(2081), 20150293. https://doi.org/10.1098/rsta.2015.0293

von Blanckenburg, F. (1999). Tracing past ocean circulation? *Science*, *286*(5446), 1862–1863.

Zhang, J., Liu, Z., Brady, E. C., Jahn, A., Oppo, D. W., Clark, P. U., et al. (2017). Asynchronous warming and oxygen isotope evolution of deep Atlantic water masses during the last deglaicaction. *Proceedings of the National Academy of Sciences*, *114*(42), 11,075–11,080. https://doi.org/10.1073/pnas.1704512114

Erratum

The originally published version of this article omitted the expanded model name abbreviated by the acronym CESM1. This error has been corrected, and this may be considered the authoritative version of record.